Step tunneling enhanced asymmetry in metal-insulator-insulator-metal (MIIM) diodes for rectenna applications

N. Alimardani and J.F. Conley, Jr.*
Department of Electrical Engineering and Computer Science
Oregon State University, Corvallis, OR, USA, 97331, *jconley@eecs.oregonstate.edu

ABSTRACT

We combine nanolaminate bilayer insulator tunnel barriers (Al_2O_3/HfO_2, HfO_2/Al_2O_3, Al_2O_3/ZrO_2) deposited via atomic layer deposition (ALD) with asymmetric work function metal electrodes to produce MIIM diodes with enhanced I-V asymmetry and non-linearity. We show that the improvements in MIIM devices are due to step tunneling rather than resonant tunneling. We also investigate conduction processes as a function of temperature in MIM devices with Nb_2O_5 and Ta_2O_5 high electron affinity insulators. For both Nb_2O_5 and Ta_2O_5 insulators, the dominant conduction process is established as Schottky emission at small biases and Frenkel-Poole emission at large biases. The energy depth of the traps that dominate Frenkel-Poole emission in each material are estimated.

Keywords: tunnel diodes, metal-insulator-metal, MIM diodes, MIIM, step tunneling, conduction mechanisms, atomic layer deposition

1. INTRODUCTION

Thin film MIM based tunneling devices are seeing renewed attention for high speed applications [1-6]. Besides rectenna solar cells [7-9], these applications include hot electron transistors [10,11] and infrared (IR) detectors [12,13]. MIM diodes have also been proposed for macroelectronics applications [14] such as backplanes for liquid-crystal displays (LCDs) [15]. We have recently shown that combining ultrasmooth amorphous metal bottom electrodes with high quality insulators deposited via atomic layer deposition allows the formation of MIM devices with well controlled quantum-mechanical tunneling [1,2]. For rectenna based solar cells as well as other potential applications of MIM diodes, highly asymmetric and non-linear current vs. voltage (I-V) behavior at low applied voltages is desired [8]. The ultrahigh frequency terahertz operation regime desired for these devices requires that the electron transport time between terminals be as short as a few femtoseconds. The standard approach to achieving high speed rectification in an MIM device is based on Fowler-Nordheim tunneling (FNT) conduction in conjunction with the use of asymmetric work function metal electrodes (metals with different work functions, $\Phi_{M1} \neq \Phi_{M2}$) to produce asymmetric, polarity dependent electron tunneling barriers [16,17]. However, the amount of asymmetry achievable using this approach is limited by the V_{bi} ($\Delta\Phi_M$) that can be obtained using practical electrodes. Here we investigate an alternative approach in which an asymmetric bilayer tunnel barrier is formed by combining two insulators with different band-gaps (E_G) and electron affinities (χ), to produce metal-insulator-insulator-metal (MI_1I_2M) devices [6], as illustrated in Figure 1.

In this work, we combine nanolaminate bilayers of Al_2O_3/HfO_2, HfO_2/Al_2O_3, Al_2O_3/ZrO_2 with asymmetric work function electrodes and demonstrate experimentally (i) that bilayer insulator tunnel barriers enable tuning of asymmetry (η_{asym}) and non-linearity (f_{NL}), (ii) that η_{asym} and f_{NL} values are sensitive to the arrangement of the individual insulator layers with respect to the larger and smaller Φ_M electrodes (e.g. $M_1I_1I_2M_2$ vs. $M_1I_2I_1M_2$), and (iii) that bilayer tunnel insulators can be arranged to either enhance or oppose (even reverse) the built-in asymmetry of the asymmetric work function electrodes. Although as illustrated in Figure 1, I-V asymmetry could in principle be enhanced through either resonant tunneling or step tunneling, we show that step tunneling – the step reduction in the minimum tunnel distance that occurs at the applied bias at which tunneling may begin to take place through only the wider band-gap insulator layer – dominates the influence of the bilayer tunnel barrier on the electrical behavior of the M_1IIM_2 devices in this study.

The selection of insulator is critical. Insulators with a large electron affinity (χ) are attractive for MIM devices as they produce small energy barriers at the metal electrodes and ideally allow FNT to occur at small applied bias (low V_{ON}). It has been suggested that Nb_2O_5 and Ta_2O_5, insulators with large χ, should be promising candidate insulators for rectenna applications [18,19]. In this work, we also investigate conduction processes in Nb_2O_5 and Ta_2O_5 and find that conduction

Next Generation (Nano) Photonic and Cell Technologies for Solar Energy Conversion IV,
edited by Oleg V. Sulima, Gavin Conibeer, Proc. of SPIE Vol. 8824, 88240S · © 2013 SPIE
CCC code: 0277-786X/13/$18 · doi: 10.1117/12.2024750

in these materials is dominated by thermal processes - Schottky emission at low bias and Frenkel-Poole emission at higher biases. Because tunneling does not appear to play a strong role in the operation of these MIM devices, it is concluded that an Nb_2O_5 / Ta_2O_5 bilayer would not be a good candidates for improving asymmetry in an MIIM device.

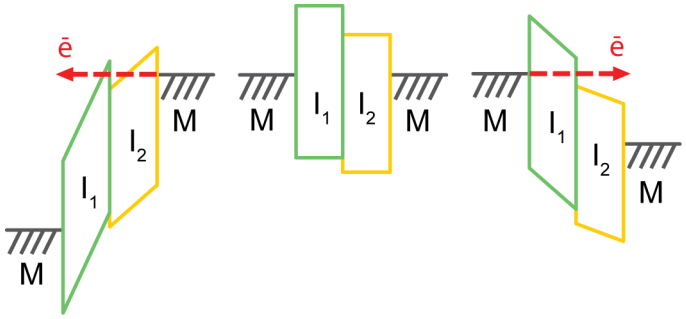

Figure 1. Energy band diagrams of *symmetric* electrode MI_1I_2M tunnel diodes, illustrating resonant tunneling (left) and step tunneling (right). For all band diagrams, the left electrode is grounded and voltage is applied to the right electrode (adapted from [20]).

2. EXPERIMENTAL DETAILS

2.1 Fabrication

MIM and MIIM diodes were fabricated on Si substrates capped with 100 nm of thermally grown SiO_2. A 150 nm thick ZrCuAlNi (ZCAN) amorphous metal bottom electrode was then deposited via DC magnetron sputtering using a $Zr_{40}Cu_{35}Al_{15}Ni_{10}$ metal target [1,2]. Insulating tunnel barriers were deposited via ALD using a Picosun SUNALE R-150B at a deposition temperature of 250 ºC. Trimethylaluminum (TMA), tetrakis (ethylmethylamino) hafnium (TDMA-Hf) tetrakis (ethylmethylamino) zirconium (TEMA-Zr), Tantalum ethoxide ($Ta_2(OC_2H_5)_{10}$) and niobium ethoxide ($Nb_2(OC_2H_5)_{10}$) were used as the metal precursors for Al_2O_3, HfO_2, ZrO_2, Ta_2O_5, and Nb_2O_5, respectively. Deionized water was used as the oxidant in all depositions. Nanolaminate insulator bilayers (HfO_2/Al_2O_3, Al_2O_3/HfO_2, or ZrO_2/Al_2O_3) were deposited in one continuous run without breaking vacuum. Top electrodes were formed by evaporating Al dots (~0.25 mm^2) through a shadow mask. To avoid any possibility of crystallization of either the ALD insulators or the ZrCuAlNi bottom electrode, all devices were studied without post-deposition annealing.

2.2 Characterization

The thickness of the insulator films on Si was measured with a J.A. Woollam WVASE32 spectroscopic ellipsometer using a Cauchy model. Optical dielectric constants were also determined with spectroscopic ellipsomtery using 10 nm thick films deposited on silicon substrates. Electrical measurements were conducted at room temperature using a probe station, a dark box, and an Agilent 4156C semiconductor parameter analyzer. The noise floor of this system is estimated to be on the order of 10^2 pA. The ZCAN bottom electrode was always held at ground with bias applied to the Al top gate. To mitigate the impact of displacement current, all I-V curves were swept from zero-bias to either the maximum positive or negative bias. I-V asymmetry, η_{asym}, is defined as negative device current divided by positive current $|I_-| / I_+$ so that $\eta_{asym} = 1$ indicates symmetric operation. Non-linearity, f_{NL}, is defined as (dI/dV) / (I/V). Band diagrams were simulated using the Boise State University Band Diagram program [21]. Materials parameters used in simulations are: electron affinity (χ) = 1.3 eV, bandgap (E_G) = 6.4 eV and relative dielectric constant (κ) = 7.6 for Al_2O_3; χ = 2.5 eV, E_G = 5.8 eV and κ = 18 for HfO_2; χ = 4 eV, E_G = 4.3 eV and κ = 25 for Nb_2O_5 [18,22]; χ = 3.75 eV, E_G = 4.4 eV and κ = 26 for Ta_2O_5 [22,23]. The work function (Φ_M) of the ZrCuAlNi and Al electrodes were determined to be 4.2 eV and 4.8 eV, respectively, as have reported in previous work [6].

3. EXPERIMENTAL RESULTS & DISCUSSION

3.1 Step tunneling in metal-insulator-insulator-metal (MIIM) diodes

Figure 2 shows (a) log (J) vs. V, (b) log (η_{asym}) vs. V, and (c) f_{NL} vs. V plots for ZrCuAlNi/Al_2O_3/HfO_2/Al $M_1I_1I_2M_2$ and ZrCuAlNi/HfO_2/Al_2O_3/Al $M_1I_2I_1M_2$ diodes. The HfO_2 and A_2O_3 layers in these devices were deposited using 32 and 28

ALD cycles, respectively. The estimated thicknesses of the bottom and top insulator layers are ~1 nm and ~2.5 nm, respectively. Included for reference are approximately 5 nm thick single insulator Al_2O_3 and HfO_2 M_1IM_2 diodes, deposited using 56 and 65 ALD cycles, respectively.

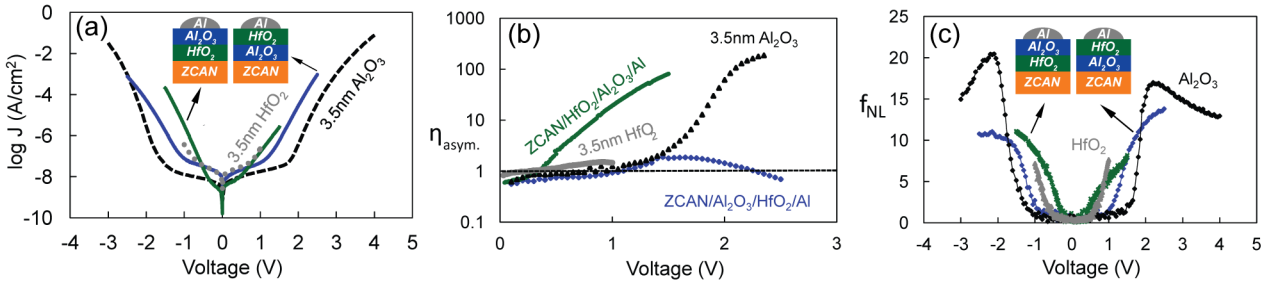

Figure 2. Plots of (a) log (J) vs. V, (b) log (η_{asym}) vs. V, and (c) f_{NL} vs. V for ZCAN/Al_2O_3/HfO_2/Al $M_1I_1I_2M_2$ and ZCAN/HfO_2/Al_2O_3/Al $M_1I_2I_1M_2$ diodes. Single layer Al_2O_3 and HfO_2 devices are included for comparison (adapted from [6]).

The inherent asymmetry of these dual insulator barriers is seen in the equilibrium band diagrams shown in Figure 3. The difference in the electrical behavior of these devices is qualitatively explained by the non-equilibrium band diagrams, which illustrate the approximate onset of step tunneling (a) at positive bias (right side) for the ZrCuAlNi/Al_2O_3/HfO_2/Al device and (b) at negative bias (left side) for the ZrCuAlNi/HfO_2/Al_2O_3/Al device. The "onset of step tunneling" refers to the applied bias at which the E_F in the electron emitting metal rises just above the E_C of the lower barrier HfO_2 so that tunneling may occur through only the larger barrier Al_2O_3 layer. It should be noted that only step tunneling is of concern to this work. As shown in Figure 2(a), the electric field required to reach resonant tunneling exceeds the breakdown strength of the constituent HfO_2 and Al_2O_3 insulators. Thus, for the insulators used in this study, resonant tunneling is not relevant.

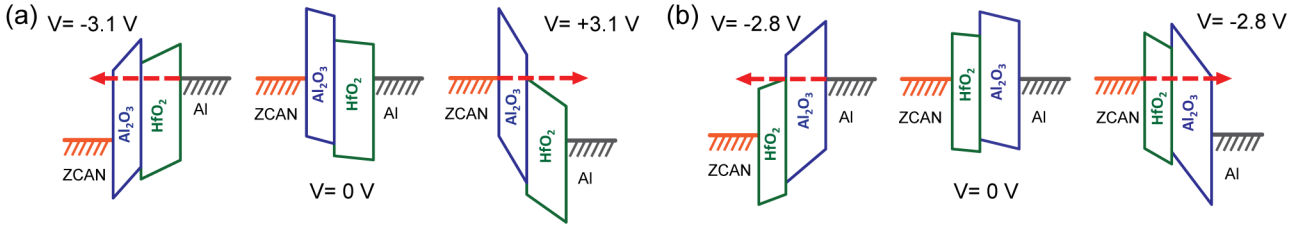

Figure 3. Energy band diagrams illustrating (a) ZCAN/Al_2O_3/HfO_2/Al $M_1I_1I_2M_2$ and (b) ZCAN/HfO_2/Al_2O_3/Al $M_1I_2I_1M_2$ diodes under negative bias (left), equilibrium (center), and positive bias (right) (adapted from [6]).

The "knee" in the log (J-V) curves of all Al_2O_3 containing devices is an indication of the onset of FNT. In FNT, J is related to V as

$$J_{FNT} = C_1 \left(\frac{V + \Delta\varphi}{S}\right)^2 exp\left(C_2\sqrt{m^*}\varphi_b^{\frac{3}{2}}\left(\frac{S}{V + \Delta\varphi_b}\right)\right), \quad (1)$$

where q is the electron charge, V is the applied bias, φ_b is the barrier height of the electrode-insulator interface from which electrons are tunneling, $\Delta\varphi$ is the difference in barrier heights between the top and bottom electrode / insulator interfaces (for single insulator layer MIM devices $\Delta\varphi = \Delta\Phi$), m^* is the effective electron mass, S is the tunnel barrier thickness, and C_1 and C_2 are constants.

Consider first the ZrCuAlNi/Al_2O_3/HfO_2/Al $M_1I_1I_2M_2$ device, in which the smaller χ Al_2O_3 layer (I_1) is adjacent to the larger Φ_{M1} ZrCuAlNi electrode. Application of approximately +3.1 V (Figure 3(a), right) brings $E_{F\text{-}ZrCuAlNi}$ to just above the $E_{C\text{-}HfO2}$ so that direct tunneling may occur from left to right through only the Al_2O_3 layer - a step reduction in the minimum required tunnel distance. For application of an opposite polarity -3.1 V bias (Figure 3(a), left) electrons tunneling from right to left at $E_{F\text{-}ZrCuAlNi}$ must pass through both insulating layers. Therefore, a larger current is expected for positive bias than for an equivalent magnitude negative applied bias and $\eta_{asym} < 1$ is expected. This expectation of $\eta_{asym} < 1$ is confirmed in Figure 2(b). Note that the asymmetry ($\eta_{asym} < 1$) for the ZrCuAlNi/Al_2O_3/HfO_2/Al device is reverse that of the single Al_2O_3 layer device ($\eta_{asym} > 1$), indicating that the asymmetry of the bilayer insulator barrier not only *opposes* that of the built-in voltage induced by $\Delta\Phi_M$, but overwhelms its impact on device operation. As indicated in Eqn. 1, the tunnel current is exponentially dependent upon $\varphi_b^{-3/2}$. Since the barrier height $\varphi_{Al\text{-}HfO2} < \varphi_{ZrCuAlNi\text{-}Al2O3}$, at higher magnitude applied biases the negative bias current (tunneling from Al) will begin to increase more rapidly than the positive bias current (tunneling from ZrCuAlNi) and it is expected that the slope of the log (η_{asym})-V plot will decrease [16]. In Figure 2(b) it is seen that for application of +4 V, the slope of the log (η_{asym})-V plot has decreased.

Next consider the *reverse insulator stack orientation* ZrCuAlNi/HfO_2/Al_2O_3/Al $M_1I_2I_1M_2$ device, in which the smaller χ Al_2O_3 layer (I_1) is now adjacent to the smaller Φ_{M2} Al electrode. With -2.8 V applied to the Al gate (Figure 3(b), left), $E_{F\text{-}Al}$ lies just above $E_{C\text{-}HfO2}$ and electrons injected from the Al (M_2) may tunnel directly through only the Al_2O_3 layer (a step reduction in tunnel distance). On the other hand, for +2.8 V applied to the Al gate (Figure 3(b), right) electrons injected from the ZrCuAlNi (M_1) must pass through both insulator layers. Therefore, a smaller current is expected at positive bias than at an equivalent magnitude negative bias so that $\eta_{asym} > 1$ is expected. This expectation is also confirmed in Figure 2(b). In this case bilayer insulator barrier *enhances* the electrode $\Delta\Phi_M$ asymmetry and η is *increased* over that of the single Al_2O_3 layer M_1IM_2 diode. Since $\varphi_{Al\text{-}Al2O3} > \varphi_{ZrCuAlNi\text{-}HfO2}$, as the magnitude of the applied bias increases, the current density will begin to increase more quickly under positive bias (injection from ZrCuAlNi) than negative bias (injection from Al) and the slope of the η_{asym}-V plot will be expected to decrease. This expectation is also confirmed in Figure 2(b).

Considering non-linearity, bilayer devices have their highest f_{NL} for the bias polarity at which the step reduction in tunneling distance occurs, as seen in Figure 2(c). Consistent with the η data, f_{NL} is highest at positive bias for the ZrCuAlNi/Al_2O_3/HfO_2/Al $M_1I_1I_2M_2$ devices, while f_{NL} is highest at negative bias for the ZrCuAlNi/HfO_2/Al_2O_3/Al $M_1I_2I_1M_2$ devices.

Overall the bilayer ZrCuAlNi/HfO_2/Al_2O_3/Al device, despite reduced η_{max} and $f_{NL\text{-}max}$ as compared to the single layer Al_2O_3 device, shows excellent low voltage characteristics with $\eta_{asym} > 10$ and $f_{NL} > 5$ at voltages as low as 0.8 V, an improvement over recent work, which has shown that insulator heterojunctions can be used to produce asymmetric I-V behavior in *symmetric metal electrode* MI_1I_2M devices in which the same metal is used for the top and bottom electrodes [5,18,24]. Maragechi et al. [24], reported $\eta_{asym} \sim 10$ at 3 V and $f_{NL} < 5$ at 0.8 V for a symmetric electrode Cr/2nm HfO_2/2nm Al_2O_3/Cr diode.

For rectenna applications, high η_{asym} and high f_{NL} at low voltage are desired. Reducing the tunnel barrier thickness can help. For example, reducing the total tunnel barrier thickness from approximately 10 nm to approximately 5 nm resulted in improved f_{NL} at small biases for single layer as well as bilayer devices [6], due primarily to the lower turn on voltages and higher conductivity for the thinner devices. However, the improvement for the bilayer devices was found to be even greater than for single layer devices. Shown in Figure 4 are J-V plots of various devices in which the total thickness of the tunnel barrier is 10 nm and consists of either (i) a single layer of Al_2O_3, (ii) a single layer of ZrO_2, or (iii) various Al_2O_3/ZrO_2 I_1/I_2 bilayers with different relative layer thicknesses. In all cases, ZrCuAlNi bottom electrode devices and Al top electrodes are used. It is seen that relative thickness of the individual insulator layers in the bilayer stack allows further tuning of electrical behavior.

In this section, it was shown that bilayer tunnel barriers can be used to effectively tune asymmetry, non-linearity, and V_{ON} in MIIM devices. In next section, the use of high χ insulators for reduced tunnel barrier height as a potential route to further improvements will be assessed.

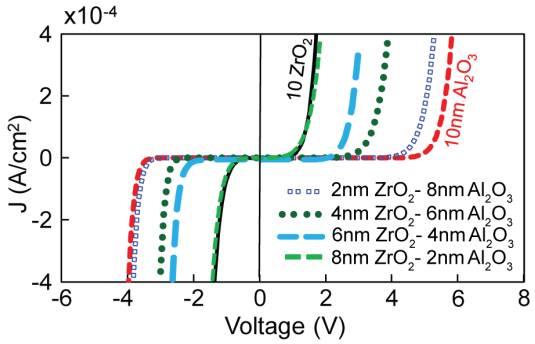

Figure 4. J-V plots for $M_1I_1I_2M_2$ diodes made with ZrCuAlNi bottom and Al top electrodes. The tunnel barrier consists of either a single layer of Al_2O_3, a single layer of ZrO_2, or various Al_2O_3/ZrO_2 I_1/I_2 bilayers. In all cases, the total thickness of the tunnel barrier is 10 nm (adapted from [20]).

3.2 Investigation of conduction mechanisms in Nb_2O_5 and Ta_2O_5 MIM diodes

Besides high asymmetry and nonlinearity, an additional requirement for rectenna applications is low V_{ON}. Assuming that operation is based on tunneling, insulators with a large electron affinity (χ) are desired to produce small energy barriers at the metal electrodes and potentially allow FNT to occur at small applied bias (low V_{ON}). It has thus been suggested that Nb_2O_5 and Ta_2O_5, insulators with large χ, should be promising candidate insulators for rectenna applications [3,18]. It has also been predicted that Nb_2O_5 / Ta_2O_5 bilayers should be promising candidate insulators for MIIM devices for rectenna applications [18,19]. Shown in Figure 5 are simulated band diagrams for a *symmetric electrode* Al/ Nb_2O_5/Ta_2O_5/Al device. It is seen that the minimum voltages required for resonant tunneling and step tunneling are predicted to be much smaller than for the Al_2O_3/HfO_2 stacks shown in Figure 3. However, as we have shown in the last section, conduction should be dominated by tunneling. In this section, the dominant conduction processes for MIM diodes made with Nb_2O_5 or Ta_2O_5 are determined.

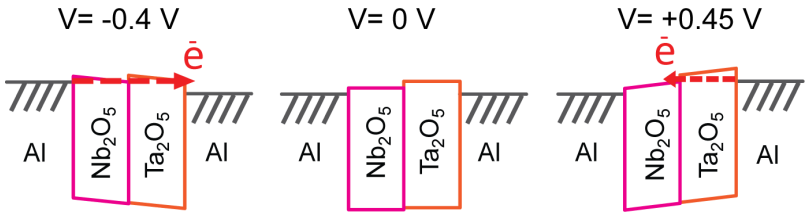

Figure 5. Simulated energy band diagrams of $Al/Nb_2O_5/Ta_2O$=/Al MI_1I_2M symmetric electrode tunnel diodes, showing step tunneling (right) and resonant tunneling (left). In all diagrams, the left electrode is grounded and voltage is applied to right electrode (adapted from [20]).

Shown in Figure 6 are log J-V plots for (a) ZCAN / 5 nm Nb_2O_5 / Al and (b) ZCAN / 5 nm Ta_2O_5 / Al M_1IM_2 devices at temperatures ranging from 300°K to 375°K. As expected based on the electron affinities and expected relative barrier heights ($\chi_{Nb2O5} > \chi_{Ta2O5}$), devices made using Nb_2O_5 show a larger current density than devices made using Ta_2O_5. The strong temperature dependence exhibited by both the Nb_2O_5 and Ta_2O_5 devices suggest the dominance of a thermal emission conduction mechanism rather than FNT.

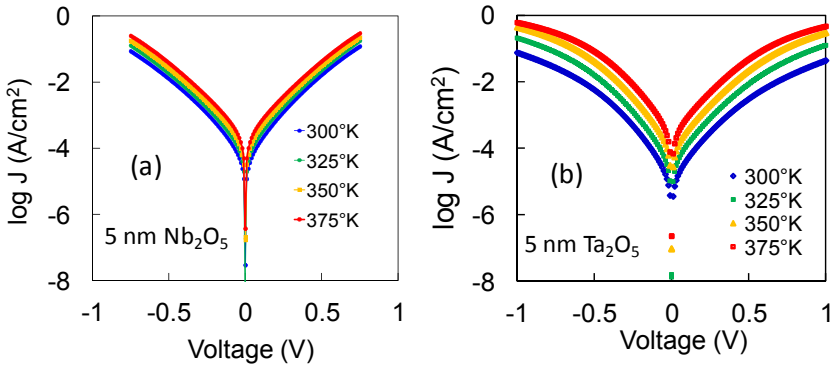

Figure 6. Log (J)-V plots as a function of temperature for (a) 5 nm thick Nb_2O_5 and (b) 5 nm Ta_2O_5 diodes.

Besides FNT and direct tunneling, possible conduction mechanisms include Schottky emission (SE), Frenkel-Poole emission (FPE), and space-charge-limited (SCL) conduction. SCL is ruled out because J does not exhibit a V^2 dependence [25]. In SE, conduction is limited by emission over a barrier and the current density, J_{SE}, has the following relationship with electric field, E [15].

$$J_{SE} = A^* T^2 \, exp\left[\frac{-q\left(\Phi_B - \sqrt{qE/4\pi\kappa_r\epsilon_0}\right)}{kT}\right], \tag{2}$$

where A^* is the effective Richardson constant, T is temperature, q is the elementary charge, Φ_B is the barrier height between the E_F of the injecting metal and the conduction band minimum of the insulator, κ_r is the optical insulator constant, ε_0 is the permittivity in vacuum, and k is Boltzmann's constant. For FPE, where conduction is limited by capture and emission from traps, the relationship between J_{FPE} and E is [15],

$$J_{FPE} = E \, exp\left[\frac{-q\left(\phi_T - \sqrt{qE/\pi\kappa_r\epsilon_0}\right)}{kT}\right], \tag{3}$$

where ϕ_T is the trap energy depth referenced to the conduction band minimum of the insulator.

To examine whether the dominant conduction process is related to SE or FPE, the room temperature J-V data from Figure 6 were replotted as ln (I/T^2) vs. $V^{1/2}$ and ln (I/V) vs. $V^{1/2}$ in Figure 7 and Figure 8, respectively. Shown in Figure 7, it was found that both the Ta_2O_5 and Nb_2O_5 devices produced linear ln (I/T^2) vs. $V^{1/2}$ curves ($R^2 > 0.999$) at low biases (0.1 to 0.3 V) at both polarities, suggesting that SE dominates in the low bias regime. At higher biases (0.75 to 1 V), both the Ta_2O_5 and Nb_2O_5 devices produced linear ln (I/V) vs. $V^{1/2}$ plots (see Figure 8), suggesting that FPE dominates at higher biases.

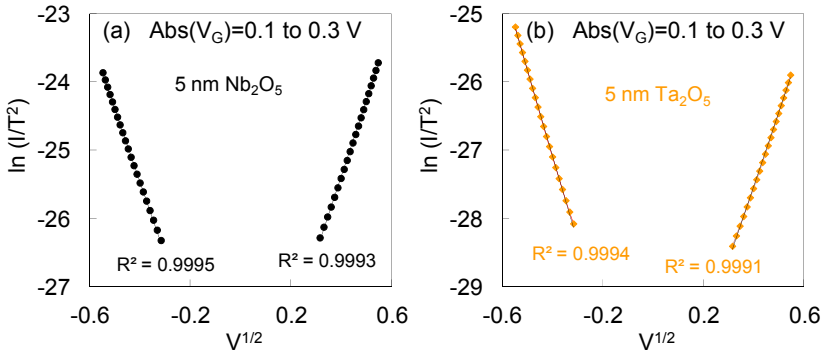

Figure 7. SE conduction plots of both (a) Nb_2O_5 and (b) Ta_2O_5 devices show linearity in the low voltage regime.

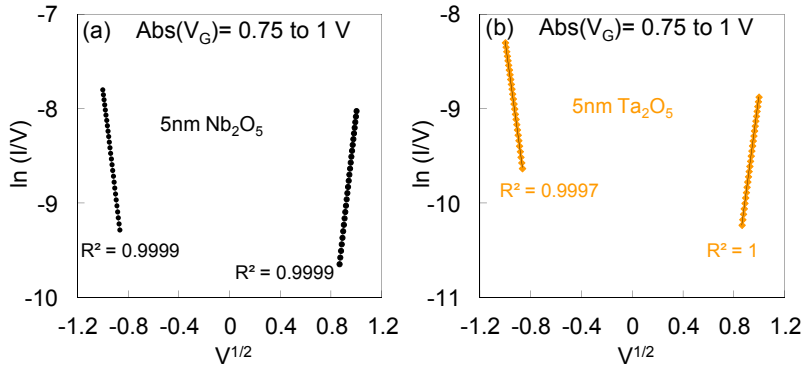

Figure 8. FPE conduction plots of both (a) Nb_2O_5 and (b) Ta_2O_5 devices show linearity in the high voltage regime.

To assess the validity of these conduction mechanism assignments, the relative dielectric constants, κ_r, of Nb_2O_5 and Ta_2O_5 were extracted from the slopes of the plots in Figure 7 and Figure 8. For Nb_2O_5, $\kappa_r = 4.7 \pm 0.3$ was extracted from the SE plot in Figure 7, and $\kappa_r = 5.5 \pm 0.1$ from FPE plot in Figure 8. For Ta_2O_5, $\kappa_r = 4.0 \pm 0.3$ was extracted from the SE plot in Figure 7 and $\kappa_r = 4.6 \pm 0.1$ from the FPE plot in Figure 8. Note that for both Nb_2O_5 and Ta_2O_5, the values of κ_r are essentially the same for both polarities. Although it is clear that all of these extracted dielectric constants are much smaller than the static dielectric constant κ of greater than 20 expected for both insulators, it is the high frequency optical dielectric constant to which they should be compared [26]. Using spectroscopic ellipsometry, the optical dielectric constant in the wavelength range of 400 – 1200 nm was measured to range from 5.5 to 6.2 for Nb_2O_5 and from 4.6 to 4.95 for Ta_2O_5. The κ_r values extracted from the FPE plots (5.5 ± 0.1 for Nb_2O_5 and 4.6 ± 0.1 for Ta_2O_5), both match well with the range of values measured optically, supporting the assignment of FPE as the dominant mechanism at higher biases. For the SE plots, the extracted κ_r values (4.7 ± 0.3 for Nb_2O_5 and 4.0 ± 0.3 for Ta_2O_5) match reasonably well but are somewhat below the range of the values measured optically, so that the designation of SE at low voltages is more tentative.

FPE may be thought of as being limited by transport through a dominant trap. The activation energy, E_a, required to escape from this trap at a given applied voltage may be extracted from Arrhenius plots of ln (I/V) vs. 1/kT as shown in Figure 9 for the 5 nm thick Nb_2O_5 devices and Figure 10 for 5 nm thick Ta_2O_5 devices. Using these field dependent E_a values, we may estimate the energy depth of the dominant trap referenced to the conduction band minimum of the insulator, ϕ_T. To account for the Schottky barrier lowering of the trap depth when a field is applied across the insulator, the obtained values of E_a are plotted vs. the square root of the voltage across the insulator, as shown in Figure 11. ϕ_T is then estimated by extrapolating to V = 0. For Ta_2O_5, ϕ_T was estimated to be 0.58+/- 0.01 eV below the conduction band minimum. For Nb_2O_5, the ϕ_T was found to be 0.60 +/- 0.04 eV below the conduction band minimum. Similar values were obtained for 10 nm thick insulators. For both Nb_2O_5 and Ta_2O_5, the extracted trap depths were the same for both positive and negative bias, further evidence that FPE is indeed dominant in this bias region.

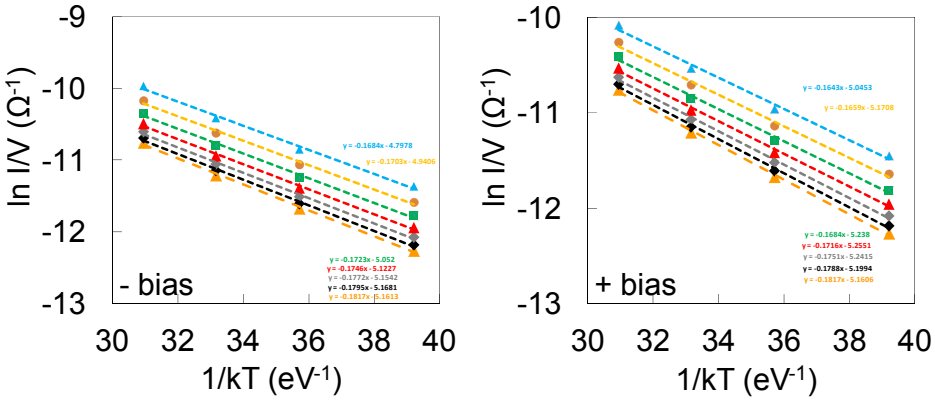

Figure 9. FPE Arrhenius plots of 5 nm thick Nb_2O_5 device at (a) negative and (b) positive bias.

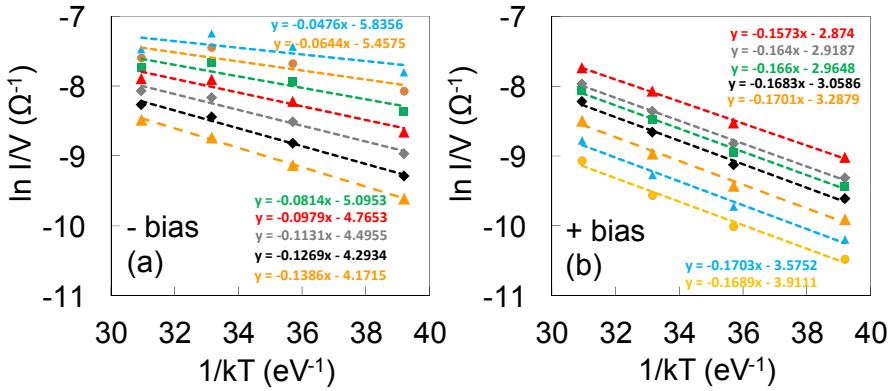

Figure 10. FPE Arrhenius plots of 5 nm thick Ta_2O_5 device at (a) negative and (b) positive bias.

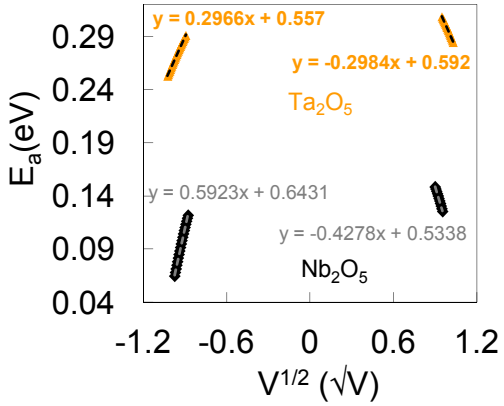

Figure 11. Plot of E_a vs. sqrt(V) for Nb_2O_5 and Ta_2O_5 diodes. The trap depth, $\phi_{T0,}$ is estimated by extrapolation to zero bias.

4. SUMMARY / CONCLUSION

Nanolaminate bilayer of insulators (each with different E_G and χ) were deposited via ALD and used to create asymmetric tunnel barrier MI_1I_2M devices in which electrons tunneling from one metal electrode to the other are presented with polarity dependent barrier shape. It was found that these bilayer tunnel barriers dominate the electrical characteristics of asymmetric metal electrode M_1IIM_2 devices. I-V asymmetry and non-linearity were shown to be sensitive to the

arrangement of the individual insulator layers with respect to the different metal electrodes ($M_1I_1I_2M_2$ vs. $M_1I_2I_1M_2$). Depending on whether the smaller χ insulator was adjacent to the smaller or larger Φ_M electrode, the bilayer insulators were arranged to either enhance or oppose (even reverse), respectively, the $\Delta\Phi_M$ induced asymmetry. In addition to placement with respect to the electrodes, the relative thickness of the insulator layers was shown to further tune electrical behavior. It was shown that these results can be qualitatively well explained by step tunneling. For the insulators used in this study, resonant tunneling is not relevant as the field required to reach resonant tunneling exceeds the breakdown strength of the constituent oxides. By combining bilayer insulator tunnel barriers with the standard method of producing asymmetry, asymmetric metal electrodes, we were able to produce excellent low voltage asymmetry and non-linearity in a ZrCuAlNi/HfO_2/Al_2O_3/Al diode exceeding both that of standard single insulator layer asymmetric electrode M_1IM_2 devices as well as symmetric electrode $M_1I_1I_2M_1$ devices.

Next, the dominant conduction mechanisms in Nb_2O_5 and Ta_2O_5 insulators deposited via ALD were investigated. Conduction in both insulators was found to be dominated by thermal emission, rather than tunneling based mechanisms. For both insulators, it was found that Schottky Emission dominates at low biases whereas Frenkel-Poole Emission dominates at larger biases. Using FPE analysis, the dominant "bulk" trap depths were estimated to be 0.58+/- 0.01 eV below the conduction band minimum for Ta_2O_5 and 0.60 ± 0.04 eV for Nb_2O_5. The fact that FNT conduction does not play a role in either Nb_2O_5 or Ta_2O_5 suggests that this insulator combination will not be able to support the step tunneling mechanism we found to improve asymmetry and reduce V_{ON} in MIIM diodes [6]. Thermal emission at high electric fields can in principle be fast (possibly of order 10s of THz as assessed from spectroscopic ellipsometry). However, FPE dominated conduction cannot provide asymmetry as the traps behave in the same manner under positive and negative bias. Although interface-dominated SE can provide low voltage asymmetry if asymmetric work function electrodes are used to produce different barrier heights, the exponential temperature dependence of SE may make it unsuitable for applications where careful temperature control is not viable. Thus, because conduction is dominated by thermal emission, ultrahigh frequency applications of Nb_2O_5 or Ta_2O_5 based MIM devices may be limited.

In conclusion, these results represent an advancement in the understanding necessary to engineer thin film MIIM tunnel devices for microelectronics and rectenna applications.

ACKNOWLEDGEMENTS

The authors acknowledge NSF (DMR-0805372 and CHE-1102637) and ONAMI for financial support, J. McGlone and Professor J.F. Wager (OSU) for sputtered ZCAN films, Ram Ravichandran for assistance with spectroscopic ellipsometry, and C. Tasker for equipment support.

REFERENCES

[1] E.W. Cowell, III, N. Alimardani, C.C. Knutson, J.F. Conley, Jr., D.A. Keszler, B.J. Gibbons, and J.F. Wager, Advanced Materials **23**, 74-78 (2011).
[2] N. Alimardani, E. W. Cowell III, J.F. Wager, J.F. Conley, Jr., et al., J. Vac. Sci. and Tech. A **30**(1), 01A113 (2012).
[3] P. Periasamy, J. J. Berry, A. A. Dameron, J. D. Bergeson, D. S. Ginley, R. P. O'Hayre, and P. A. Parilla, Adv. Mater. **23**(7), 3080 (2011).
[4] K. Choi, F. Yesilkoy, G. Ryu, S.H. Cho, N. Goldsman, M. Dagenais, and M. Peckerar, IEEE Trans. Elec. Dev. **58**(10), 3519 (2011).
[5] P. Maraghechi, A. Foroughi-Abari, K. Cadien, and A.Y. Elezzabi, Appl. Phys. Lett. **100**, 113503 (2012).
[6] N. Alimardani and J. F. Conley, Jr., Appl. Phys. Lett. **102**, 143501 (2013).
[7] R. Corkish, M. A. Green, T. Puzzer, Solar Energy, **73**, 6, 395-401 (2002).
[8] N. M. Miskovsky, P. H. Cutler, A. Mayer, B. L. Weiss, B. Willis, T. E. Sullivan, P. B. Lerner, J. Nanotechnol. **2012**, 1-19 (2012).
[9] S. Joshi and G. Moddel, Appl. Phys. Lett. **102**, 083901 (2013).
[10] S. Vaziri, G. Lupina, C. Henkel, A. D. Smith, M. Ostlling, J. Dabrowski, G. Lippert, W. Mehr, and M. C. Lemme, Nano Lett. **13**(4), 1435 (2013).
[11] B. D. Kong, C. Zeng, D. K. Gaskill, K. L. Wang, and K. W. Kim, Appl. Phys. Lett. **101**, 263112 (2012).

[12] P.C.D. Hobbs, R.B. Laibowitz, F.R Libsch, N.C. LaBianca, and P.P. Chiniwalla, Opt. Exp. **15**(25), 16376 (2007).
[13] P. C. D. Hobbs, R. B. Laibowitz, and F. R. Libsch, Appl. Opt. **44**(32), 6813 (2005).
[14] W. den Boer, *Active Matrix Liquid Crystal Displays* (Elsevier, Amsterdam, 2005), pp. 43–47.
[15] S. M. Sze and K. K. Ng, *Physics of Semiconductor Devices*, 3rd Ed. (Hoboken, NJ: Wiley-Interscience, 2007).
[16] J.G. Simmons, J. Appl. Phys. **34**(9), 2581 (1963).
[17] H. Ekurt, A. Hahn, J. Appl. Phys. **51**, 1686 (1980).
[18] S. Grover and G. Moddel, Sol. Sta. Elec. **67**, 94 (2012).
[19] E. I. Hashem, N. H. Rafat, E. A. Soliman, IEEE J. Quan. Elec. **49**(1), 72 (2013).
[20] J. F. Conley, Jr. and N. Alimardani, *Chapter 6 in Rectenna Solar Cells* (Springer, New York, 2014).
[21] R. G. Southwick III, A. Sup, A. Jain, and W. B. Knowlton, IEEE Trans. Dev. and Mater. Rel. **11**(2), 236 (2011).
[22] J. Robertson, J. Vac. Sci. Technol. B **18**, 1785 (2000).
[23] K. Kukli, J. Ihanus, M. Ritala, and M. Leskelä, J. Electrochem. Soc. **144**(1), 300 (1997).
[24] P. Maraghechi, A. Foroughi-Abari, K. Cadien, and A. Y. Elezzabi, Appl. Phys. Lett. **99**, 253503 (2011).
[25] A. Rose, Phys. Rev. **97**, 1538 (1955).
[26] J. Frenkel, Phys. Rev. **54**, 647 (1938).